Supporting Information

Microwave Induced Plasma Synthesis of Defect-Rich, Highly Ordered Porous Phosphorus-Doped Cobalt Oxides for Overall Water Electrolysis

*Yuan Wang,[1] Hamidreza Arandiyan,[2] Xianjue Chen,[1] Tingwen Zhao,[1] Xin Bo,[1] Zhen Su,[1] and Chuan Zhao[1]**

[1]School of Chemistry, Faculty of Science, The University of New South Wales, Sydney, New South Wales 2052, Australia

[2]Laboratory of Advanced Catalysis for Sustainability, School of Chemistry, The University of Sydney, Sydney 2006, Australia

AUTHOR INFORMATION

Corresponding Author

Prof. Chuan Zhao

E-mail: chuan.zhao@unsw.edu.au (C.Z.)

Experimental Section

***Synthesis of 3D Co_3O_4/CP and Co_3O_4/CP*:** Poly(methyl methacrylate) (PMMA) solution was prepared according to our previous published work.[1-3] PMMA microspheres were assembled on a carbon plate (CP, 5×20 mm) by immersing the CP vertically in a PMMA solution and placing it in an oven at 60 °C for 24 h. The resulted PMMA/CP was then impregnated in a cobalt nitrate hydrate solution (20 mmol/L) for 3 h, followed by drying at 80 °C for 12 h, and calcination at 450 °C for 3 h (at a rate of 1 °C/min). Co_3O_4/CP was synthesized by directly impregnating CP in a cobalt precursor without a PMMA assembly step, followed by the same drying and calcination steps.

***Synthesis of 3D Co:Pi/CoO_x/CP and 3D CoO_x/CP*:** The 3D Co_3O_4/CP electrode obtained by the above method was placed in a round bottom flask together with 50 mg of red phosphorus powder. The flask was sealed and vacuumed and then placed in a microwave oven for 20, 30 and 40 s. After rinsing with water to remove the residual phosphorus (Figure S20), the 3D Co:Pi/CoO_x/CP electrode was obtained. The 3D CoO_x/CP was prepared in a similar manner without red phosphorus powder.

Electrochemical measurements: The electrocatalytic performance was performed with an electrochemical workstation (CHI 760) in a three-electrode cell. The saturated calomel electrode (SCE) was used as a reference electrode, while a Pt plate and a carbon plate were used as the counter electrode for OER and HER, respectively. As-prepared cobalt catalysts have a mass loading of 3 mg cm^{-2} determined by Inductively coupled plasma mass spectrometry (ICP-MS). The linear sweep voltammetry (LSV) was recorded in 1.0 M KOH solution at room temperature with a scan rate of 5 mV s^{-1}. 90% of iR-compensation was applied to the polarization curves based on resistance measured by electrochemical workstation. All the potentials in electrochemical measurements were normalised to a reversible hydrogen electrode

(RHE). Overpotential (η) is estimated from the abscissa of the LSV curves, for OER in alkaline: η (V) = E – 1.23 V, and for HER in alkaline: η (V) = E – 0.0 V.

An example of estimating the onset overpotential and overpotential at a current density of 100 mA cm^{-2} of 3D Co:Pi/CoO_x/CP catalyst is shown in Figure S9.

Measurement of electrochemical active surface area

The determination of the ECSA was realised from the double layer capacitance (*C*DL) of the electrode, as described by others.[4-5] The scan-rate-dependent charging current density (i_c) were measured in the non-faradaic region using CV curves at selected scan rates at 5, 10, 20, and 30 mV s^{-1}. The double layer charging current density was increased as expected due to the gradual increase in the scan rates. The relationship between the double layer i_c and the scan rate (v) is given in eqn (1).

$$i_c = vC_{DL} \quad (1)$$

Hence, the plot of double layer charging current (i_c) against scan rate (v) yielded a straight line, the slope of which is a direct measure of the double layer capacitance of the electrode. The C_{DL} can be converted to ECSA via the roughness factor (R) obtained by eqn (2).

$$R = C_{DL}/C_{DLRef} \quad (2)$$

Where C_{DLRef} is the double layer capacitance of the flat surface of the electrode. The ECSA is achieved by using the geometric surface area multiply by the roughness factor. Details of the calculation values (C_{DL}) are provided in Figure S15 and Table S1.

Faradaic efficiency

The Faradaic efficiency of OER was measured by rotating ring disk electrode (RRDE) method. The 3D Co:Pi/CoO_x/CP catalyst ink was dropped on the glassy carbon disk (5 mm in diameter) and allowed to dry in air under the rotating operation to guarantee a uniform distribution. The 1 M KOH electrolyte was purged with O_2 for 30 min before the test. Then

the potential of the Pt ring was set at 1.40 V vs. RHE to oxidize the peroxide intermediates formed at the 3DIO-$LaCoO_{3-x}$ surface. LSV scan from 1 to 1.7 V was applied to the disk for the purpose of activating of 3DIO-$LaCoO_{3-x}$ catalyst. Furthermore, the electrolyte was purged with N_2 for 30 min. After that, the disk current was held constant at 173 µA to undergo continuously OER while a ring potential of 0.4 V was applied to reduce the generated O_2 from water oxidation on the disk. The Faradaic efficiency was then calculated by eqn (3).

$$\frac{j_{ring}}{j_{disk} \times N} \times 100\% \qquad (3)$$

Where j_{ring} and j_{disk} are the current on the ring and disk, respectively, and N is the collection efficiency of the RRDE.

Transfer coefficient and exchange current density

The transfer coefficient α can be derived from the Tafel slope: b = 2.303 RT/ (αF): where b is the Tafel slope, R is the gas constant (8.314 J K^{-1} mol^{-1}), T is temperature (297 K), and F is the Faraday constant 96485 C mol^{-1}.[6-7] The exchange current density is another important metric that is often used to estimate the intrinsic electrocatalytic performance. It corresponds to the current density exchanged across the interface of the electrode at overpotential = 0 V.[8] The calculated transfer coefficient and exchange current density are listed in Table S2. A higher transfer coefficient and exchange current density value indicate better electrocatalytic activity.

Characterization: The XRD patterns were obtained on the PANalytical Empyrean II, in which cobalt was used as a source. All XRD patterns were converted to copper source XRD patterns using HighScore software. The XPS spectra were measured using a Thermo ESCALAB250i XPS using a monochromatic Al Kalpha soft X-ray source. Morphological studies were performed on SEM and HRTEM by FEI Nova NanoSEM 450 FE-SEM and JEOL JEM-F200

Multi-Purpose FEG-S/TEM, respectively. The BET surface area of the samples was carried out by a Micrometritics-TriStar II 3020. Before the analysis, the samples were preheated at 150 °C for 3 h to remove moisture. The EPR spectra were performed at 120 K using a Bruker EMX X-Band ESR spectrometer under a liquid Nitrogen cooling system. The contact angle with water was measured by the sessile drop method using Rame–Hart 100-00 goniometry. Three different points were measured on three different regions of the catalyst surface for averaging.

In-situ Raman measurements: The in-situ Raman was measured on a Renishaw inVia Raman Microscope (using 514 nm Argon ion laser with 1800 l/mm grating). The screen-printed three-electrode chip composed of Au working electrode and counter electrode and Ag reference electrode was applied for in-situ Raman measurements. The catalysts are deposited on the working electrode, and the potential is applied from 0.1 to 0.7 V vs Ag. The electrochemical performance was recorded at the same time by an electrochemical workstation (CHI 760).

Table S1. The specific surface area and double layer capacitance (C_{dl}) of the samples.

Catalysts	Specific Surface Area by BET[a]	C_{dl}[b]	ECSA
	$m^2\ g^{-1}$	$mF\ cm^{-2}$	cm^2
3D Co_3O_4/CP	25.9	0.15	1.28
3D CoO_x/CP	23.8	0.29	1.65
3D Co:Pi/CoO_x/CP	21.3	0.28	2.34

Table S2. The Tafel slope, transfer efficient and exchange current density of HER and OER.

Catalysts	OER			HER		
	Tafel Slope	Transfer Efficient	Exchange current density	Tafel Slope	Transfer Efficient	Exchange current density
	$mV\ dec^{-1}$		$\mu A\ cm^{-2}$	$mV\ dec^{-1}$		$\mu A\ cm^{-2}$
3D Co_3O_4/CP	103	0.57	1.21	60	0.98	7.05
3D CoO_x/CP	104	0.56	4.65	55	1.07	8.62
3D Co:Pi/CoO_x/CP	78.0	0.76	7.72	36	1.64	12.6

Figure S1. Illustration of microwave-induced plasma strategy for phosphorus doping experiment.

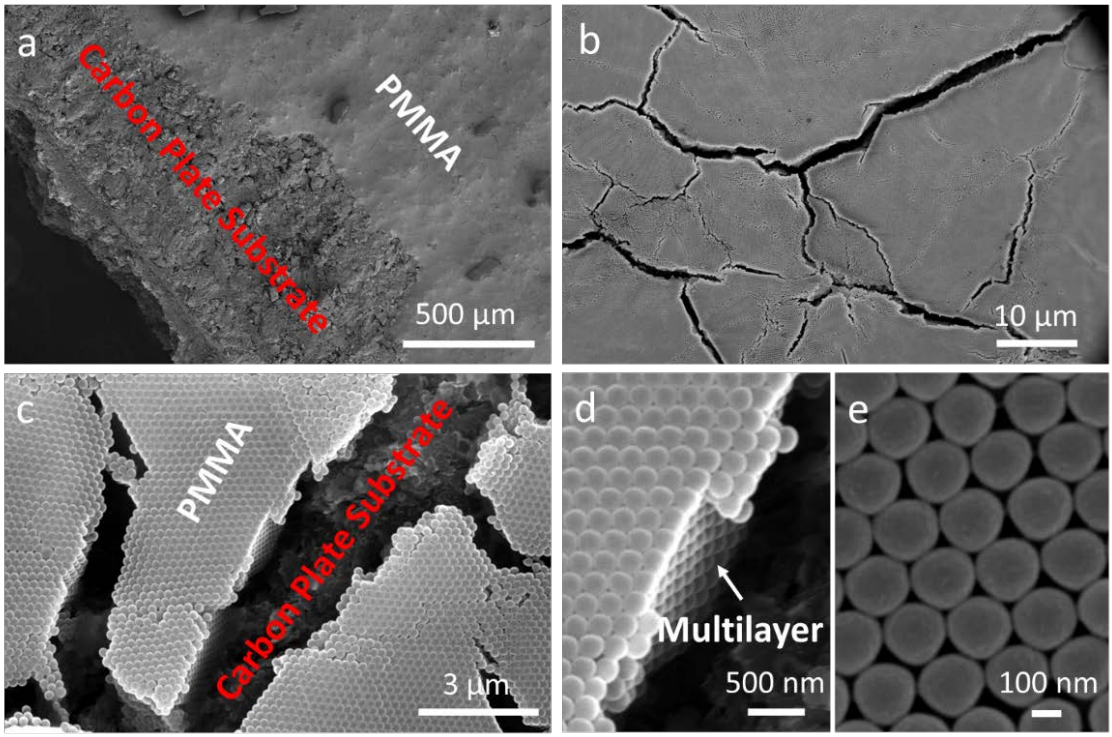

Figure S2. SEM images of PMMA template on carbon plate (CP) substrate in different magnifications.

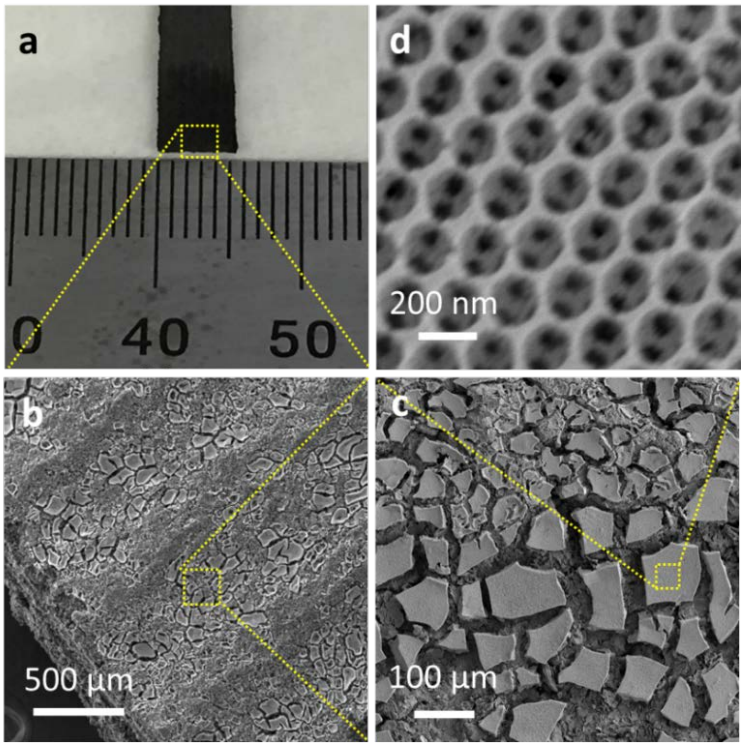

Figure S3. (a) Photo of 3D Co_3O_4/CP, (b-d) SEM images of 3D Co_3O_4/CP in different magnifications.

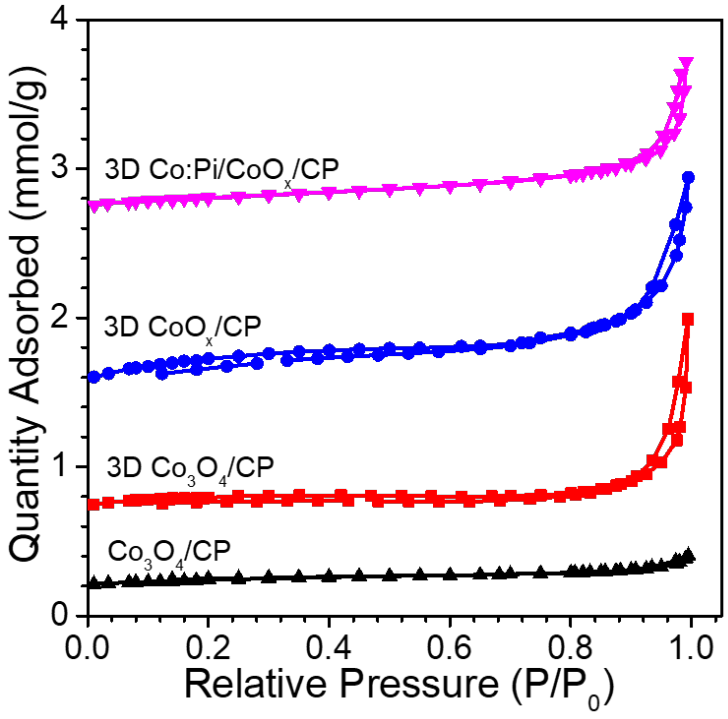

Figure S4. N_2 adsorption-desorption isotherm of Co_3O_4/CP, 3D Co_3O_4/CP, 3D CoO_x/CP and 3D Co:Pi/CoO_x/CP.

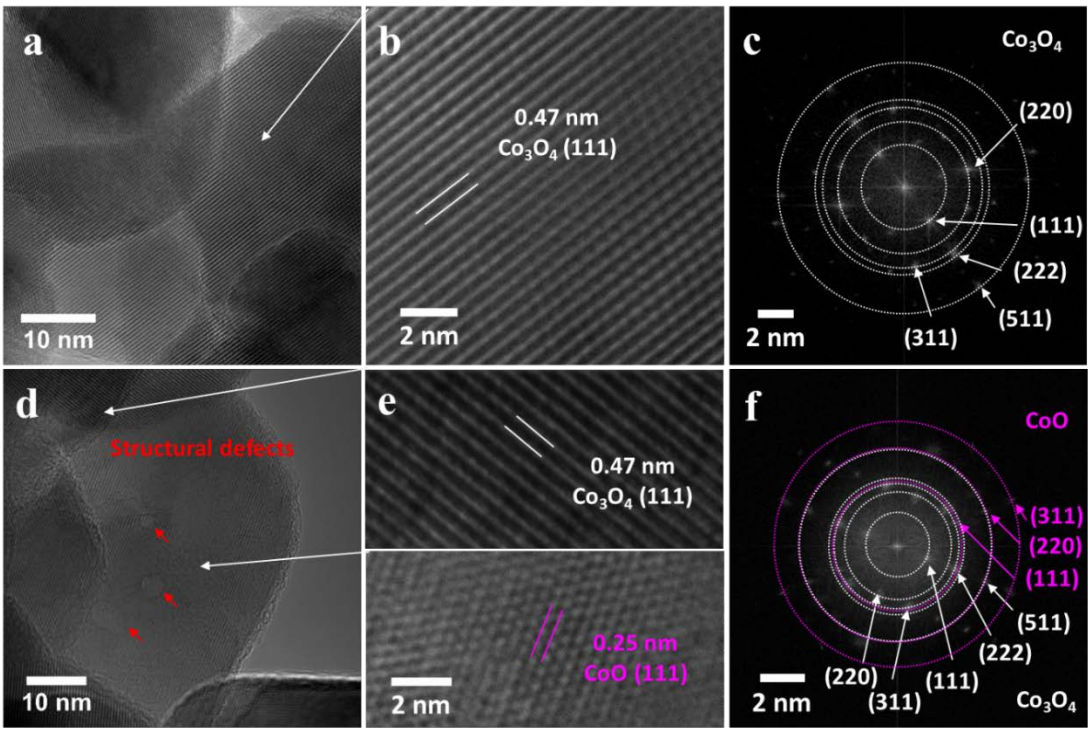

Figure S5. (a, b) HRTEM images and (c) FFT of 3D Co_3O_4/CP, (d, e) and (f) FFT of 3D CoO_x/CP.

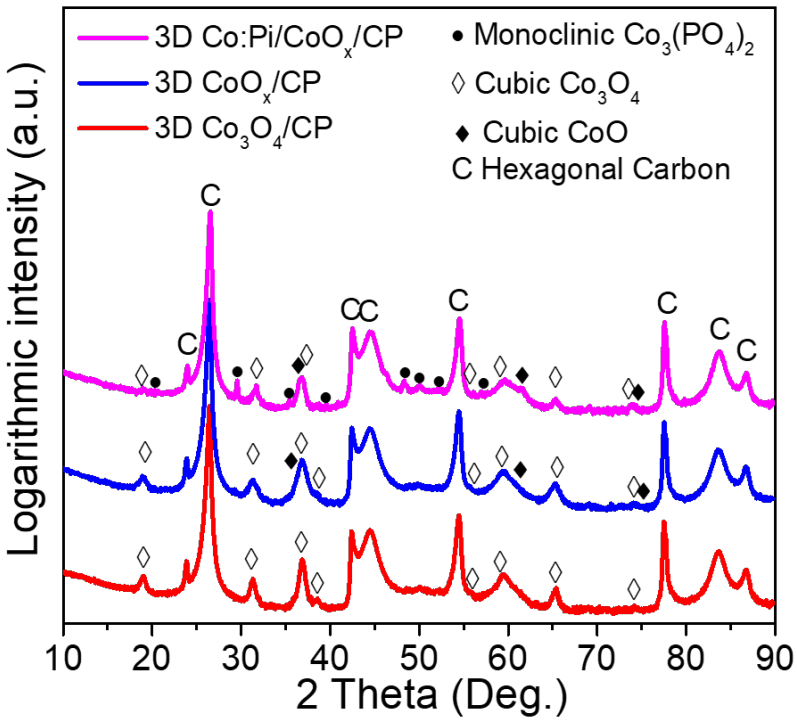

Figure S6. XRD patterns of 3D Co_3O_4/CP, 3D CoO_x/CP, 3D Co:Pi/CoO_x/CP with the carbon plate substrate.

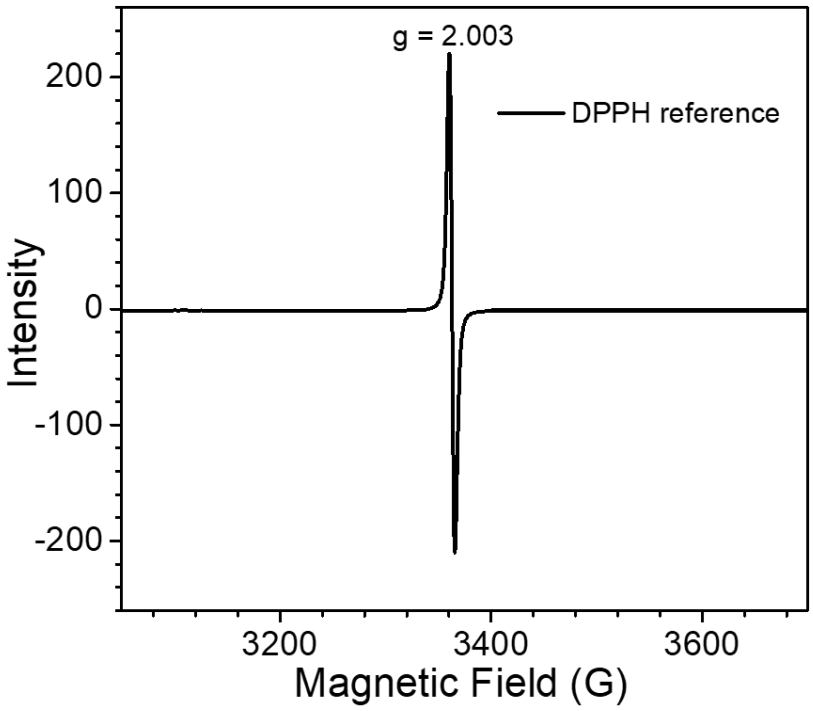

Figure S7. EPR signal of DPPH at 120 K.

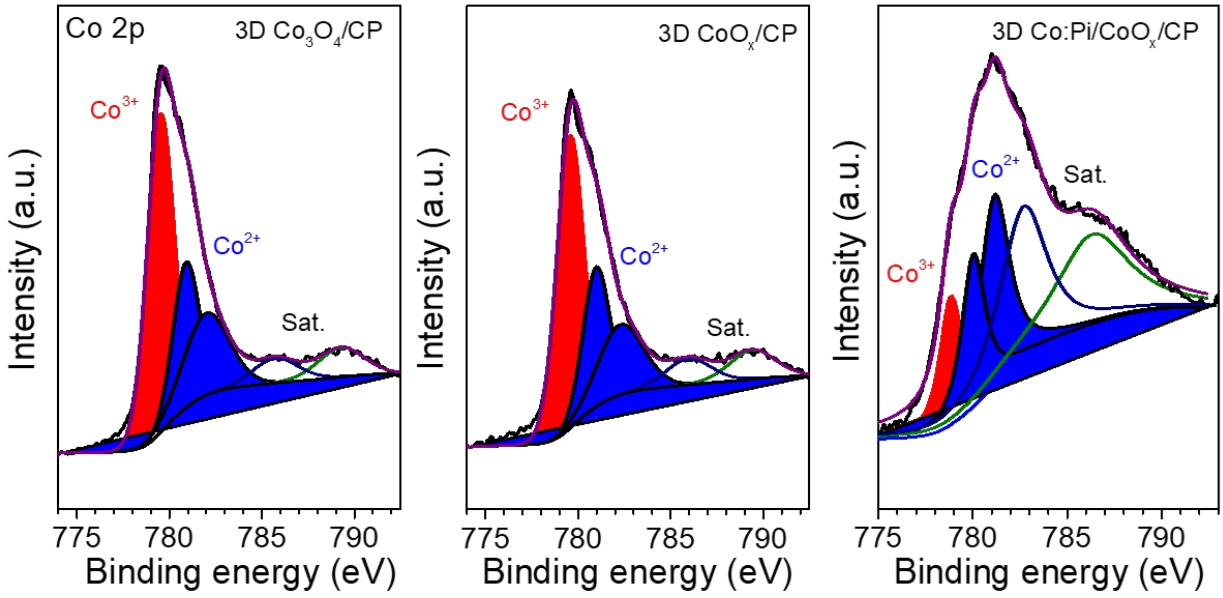

Figure S8. XPS profiles of Co 2p.

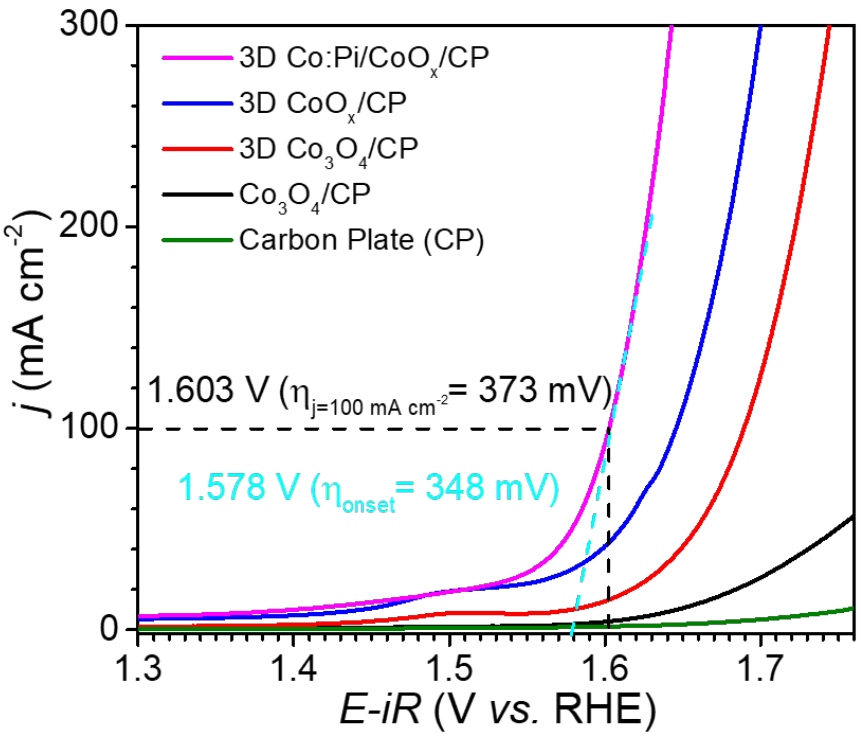

Figure S9. Estimating overpotential (η) of 3D Co:Pi/CoO_x/CP vis LSV curve.

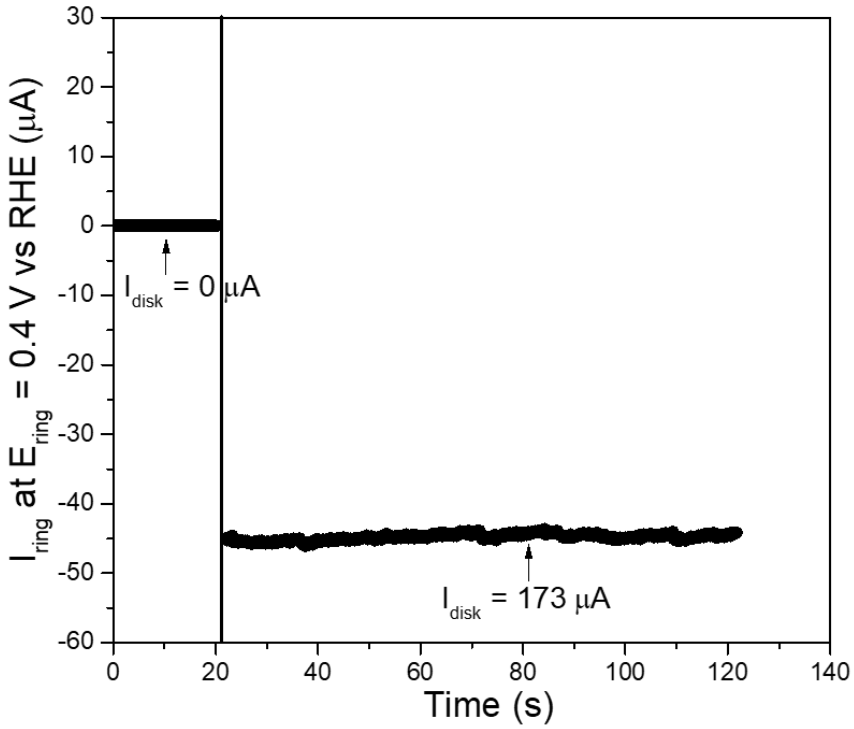

Figure S10. Ring current of 3D Co:Pi/CoO_x/CP on an RRDE (1600 rpm) in N_2-saturated 1M KOH solution (ring potential 0.40 V).

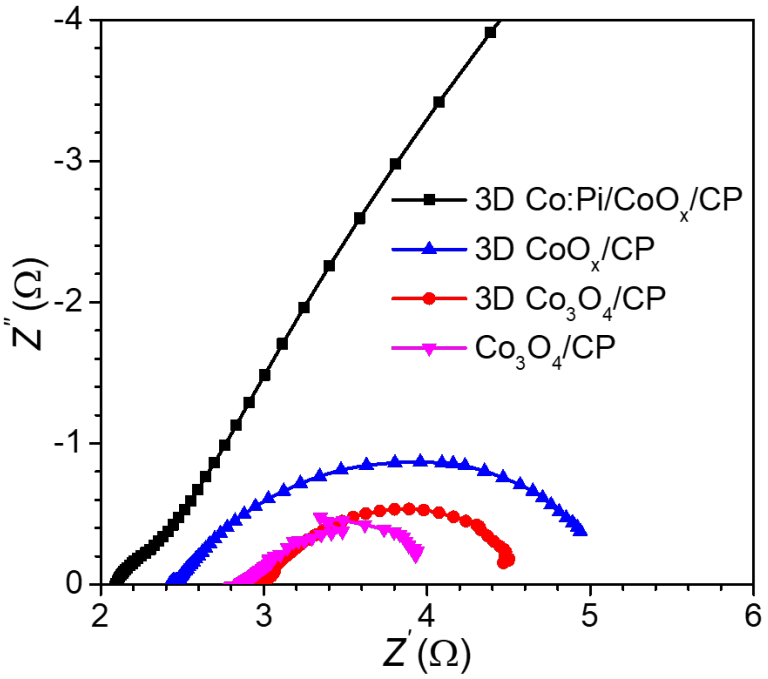

Figure S11. Nyquist plots of electrochemical impedance spectra.

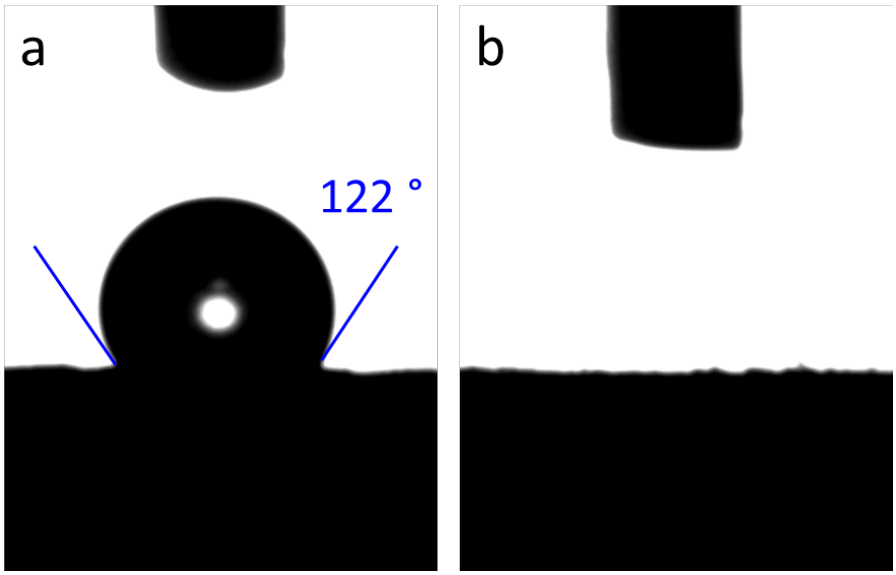

Figure S12. Contact angle measurements of (a) Co_3O_4/CP and (b) 3D Co_3O_4/CP.

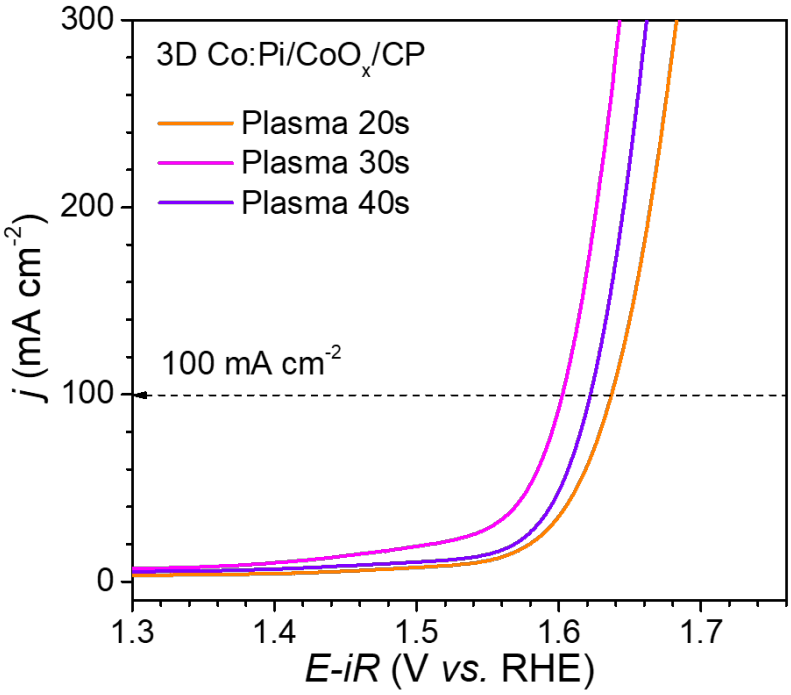

Figure S13. LSV curves of 3D Co:Pi/CoOx/CP prepared with different plasma treatment times including 20s, 30s and 40s.

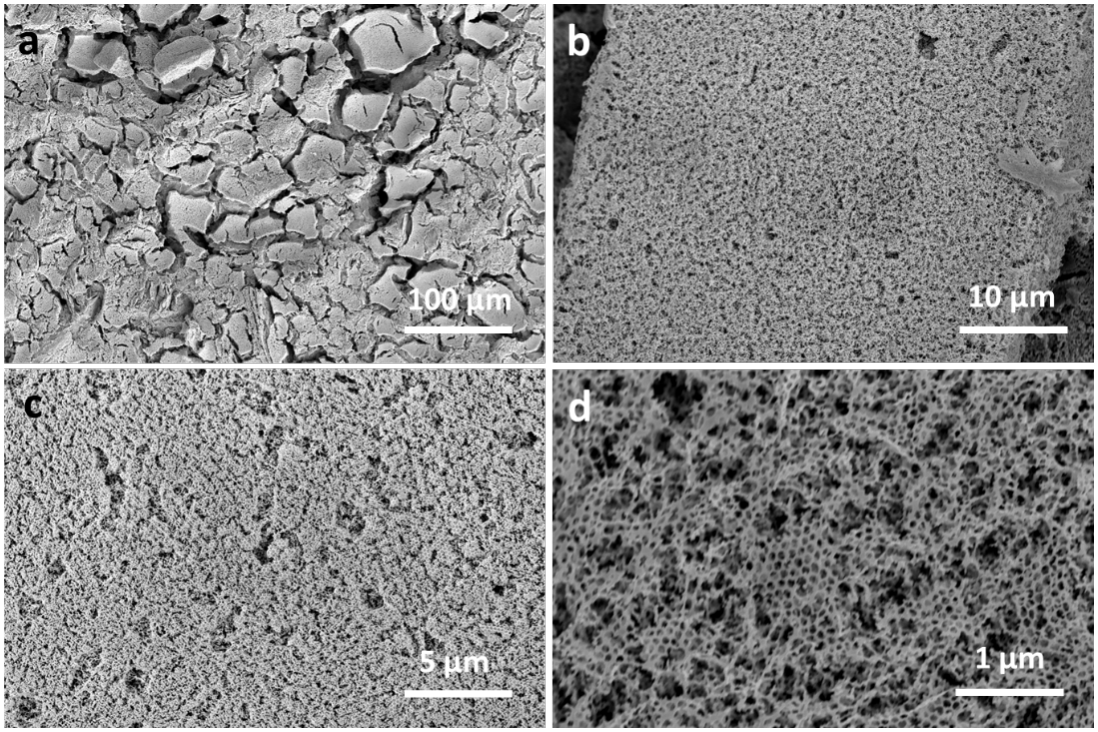

Figure S14. SEM images of aged 3D Co:Pi/CoOx/CP after long term stability test for 100 h.

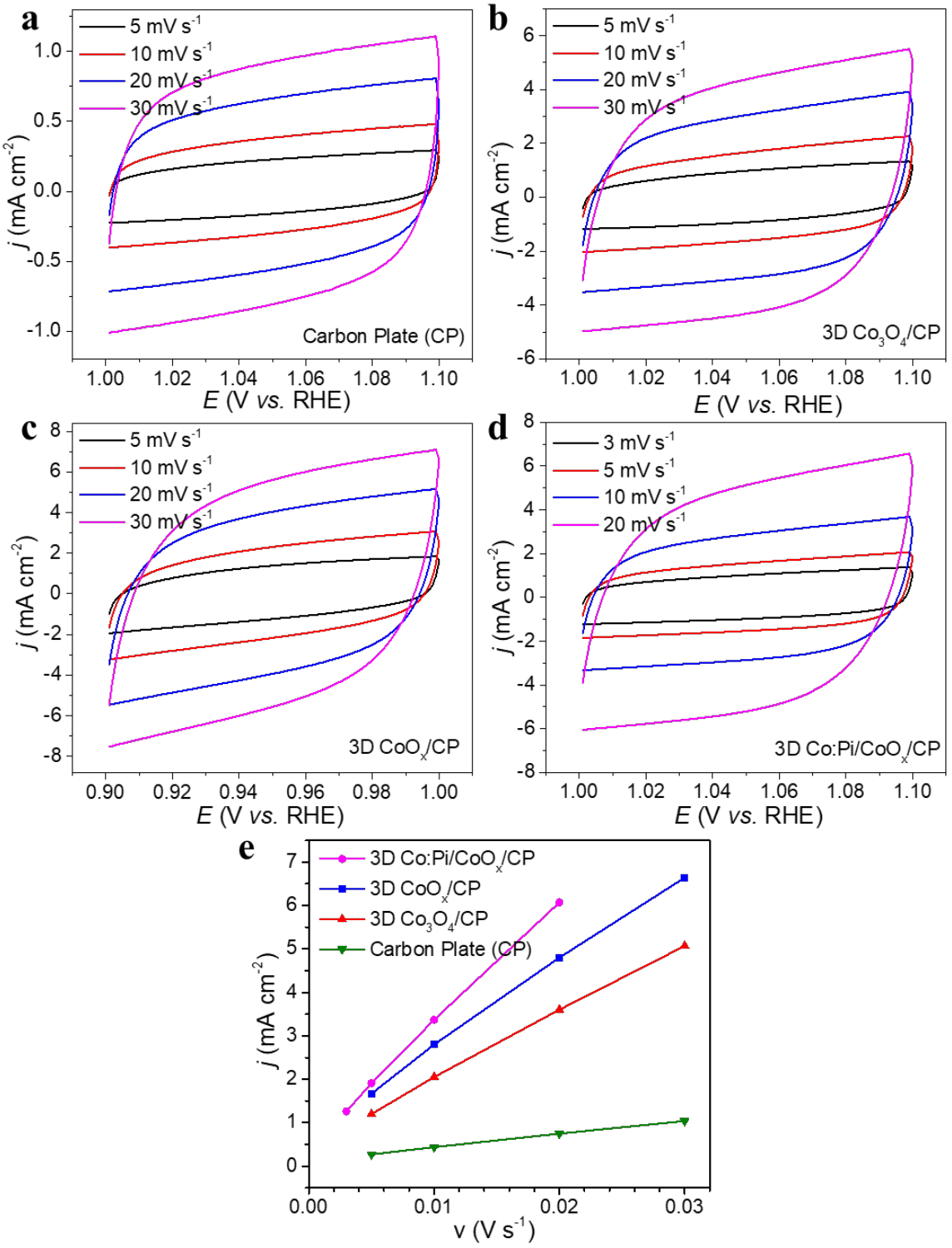

Figure S15. CV response of (a) Carbon Plate (CP), (b) 3D Co_3O_4/CP, (c) 3D CoO_x/CP and (d) 3D Co:Pi/CoO_x/CP at scan rates of 5, 10, 20, and 30 mV s^{-1}, (e) the plot of double layer charging current density *vs* scan rates for determining the double layer capacitance (C_{DL}).

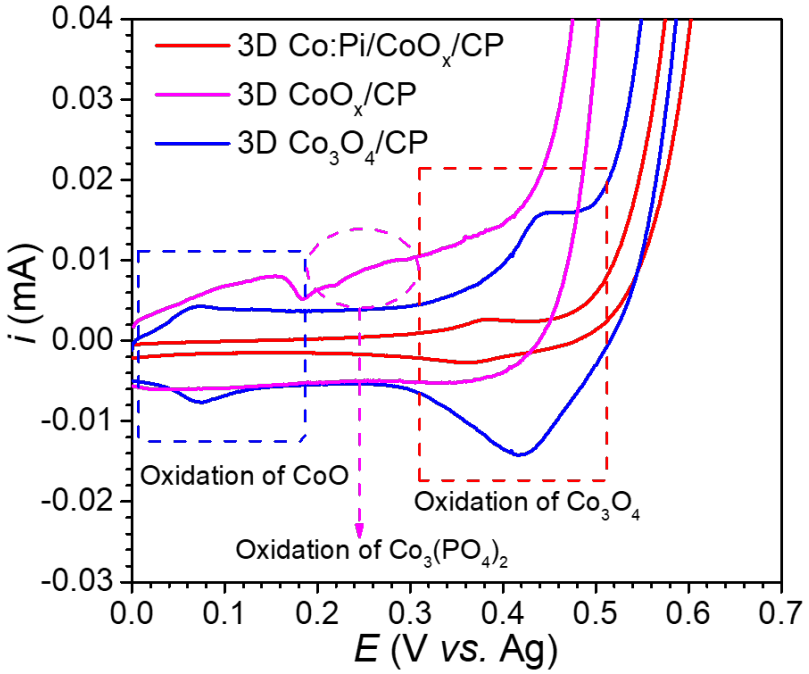

Figure S16. CV curves under in-situ Raman test, partial enlargement of redox potential.

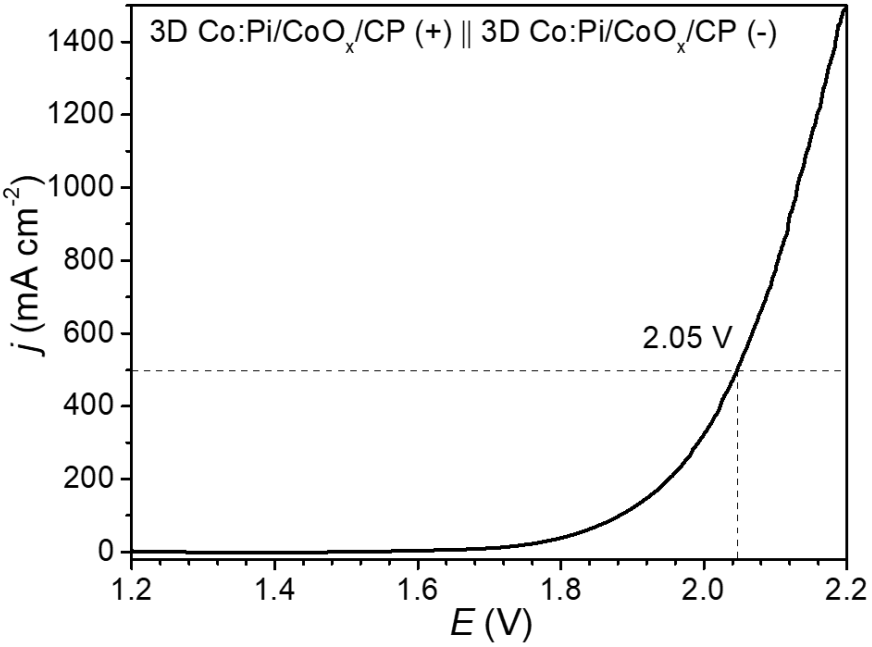

Figure S17. LSV curve obtained in two electrode cell using the 3D Co:Pi/CoO$_x$/CP as both the anode and cathode with 90% iR compensation.

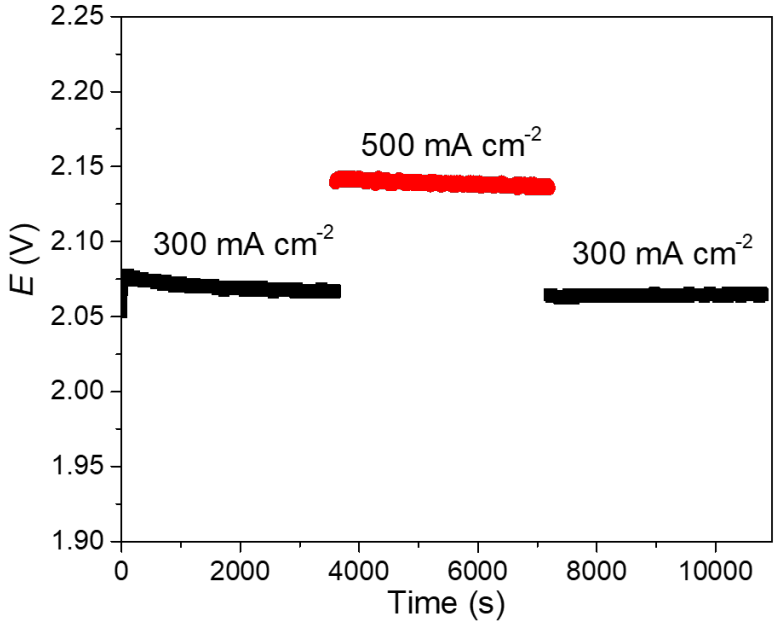

Figure S18. Chronopotentiometric curves obtained with the 3D Co:Pi/CoO_x/CP anode and cathode under the applied current density of 300 and 500 mA cm^{-2}.

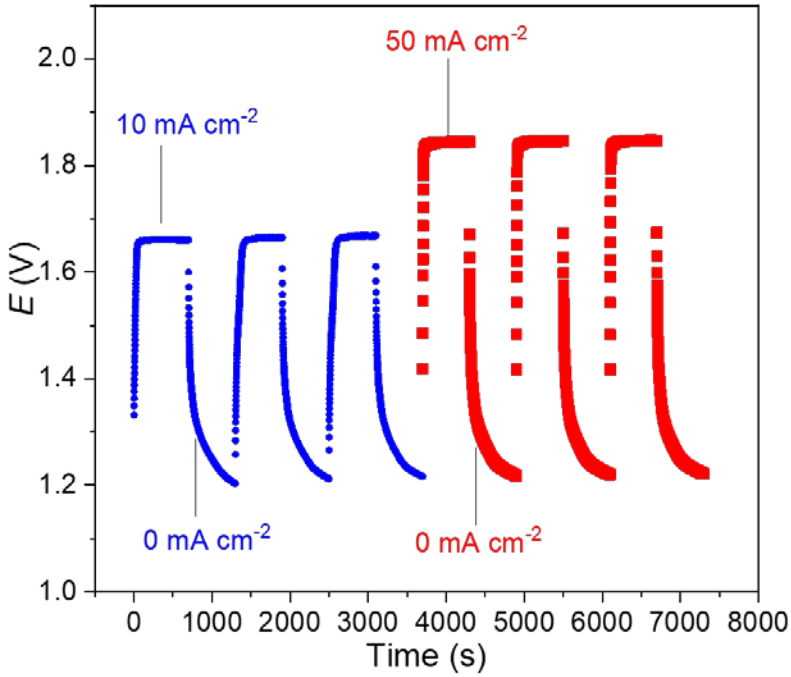

Figure S19. Chronopotentiometric curves obtained with the 3D Co:Pi/CoO_x/CP anode and cathode under the applied current density of 0, 10 and 50 mA cm^{-2}.

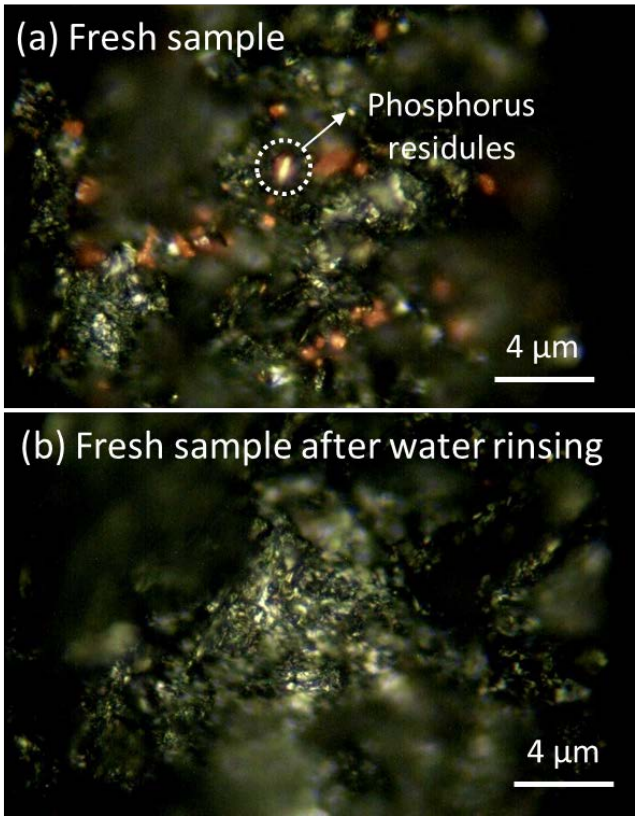

Figure S20. Raman images of the fresh sample and 3D Co:Pi/CoO_x/CP sample after water rinsing. The phosphorus residual on the surface of the electrode can be easily rinsed by water.

References

1. Wang, Y.; Arandiyan, H.; Scott, J.; Dai, H.; Amal, R., Hierarchically Porous Network-Like Ni/Co3o4: Noble Metal-Free Catalysts for Carbon Dioxide Methanation. *Advanced Sustainable Systems* **2018**, 1700119-n/a.

2. Wang, Y.; Arandiyan, H.; Tahini, H. A.; Scott, J.; Tan, X.; Dai, H.; Gale, J. D.; Rohl, A. L.; Smith, S. C.; Amal, R., The Controlled Disassembly of Mesostructured Perovskites as an Avenue to Fabricating High Performance Nanohybrid Catalysts. *Nature Communications* **2017**, *8*, 15553.

3. Wang, Y.; Arandiyan, H.; Scott, J.; Akia, M.; Dai, H.; Deng, J.; Aguey-Zinsou, K.-F.; Amal, R., High Performance Au–Pd Supported on 3d Hybrid Strontium-Substituted Lanthanum Manganite Perovskite Catalyst for Methane Combustion. *ACS Catal.* **2016**, *6*, 6935-6947.

4. Anantharaj, S.; Jayachandran, M.; Kundu, S., Unprotected and Interconnected Ru0 Nano-Chain Networks: Advantages of Unprotected Surfaces in Catalysis and Electrocatalysis. *Chem. Sci.* **2016**, *7*, 3188-3205.

5. Xu, Z.; Li, W.; Wang, X.; Wang, B.; Shi, Z.; Dong, C.; Yan, S.; Zou, Z., Novel Cobalt Germanium Hydroxide for Electrochemical Water Oxidation. *ACS Appl. Mater. Interfaces* **2018**, *10*, 30357-30366.

6. Gomez Vidales, A.; Choi, K.; Omanovic, S., Nickel-Cobalt-Oxide Cathodes for Hydrogen Production by Water Electrolysis in Acidic and Alkaline Media. *Int. J. Hydrogen Energy* **2018**, *43*, 12917-12928.

7. Vidales, A. G.; Dam-Quang, L.; Hong, A.; Omanovic, S., The Influence of Addition of Iridium-Oxide to Nickel-Molybdenum-Oxide Cathodes on the Electrocatalytic Activity

Towards Hydrogen Evolution in Acidic Medium and on the Cathode Deactivation Resistance. *Electrochim. Acta* **2019**, *302*, 198-206.
8. Voiry, D.; Chhowalla, M.; Gogotsi, Y.; Kotov, N. A.; Li, Y.; Penner, R. M.; Schaak, R. E.; Weiss, P. S., Best Practices for Reporting Electrocatalytic Performance of Nanomaterials. *ACS Nano* **2018**, *12*, 9635-9638.